European Journal of Pharmaceutical Sciences xxx (2012) xxx–xxx

Contents lists available at SciVerse ScienceDirect

European Journal of Pharmaceutical Sciences

journal homepage: www.elsevier.com/locate/ejps

Lymphatic trafficking kinetics and near-infrared imaging using star polymer architectures with controlled anionic character

Taryn R. Bagby [a], Shaofeng Duan [a], Shuang Cai [a], Qiuhong Yang [a], Sharadvi Thati [a], Cory Berkland [a], Daniel J. Aires [b], M. Laird Forrest [a,*]

[a] Department of Pharmaceutical Chemistry, University of Kansas, Lawrence, KS, USA
[b] Division of Dermatology, Dept. of Internal Medicine, University of Kansas Medical Center, Kansas City, KS, USA

ARTICLE INFO

Article history:
Received 20 December 2011
Received in revised form 16 April 2012
Accepted 17 April 2012
Available online xxxx

Keywords:
Lymphatics
Imaging
Polymer trafficking

ABSTRACT

Targeted lymphatic delivery of nanoparticles for drug delivery and imaging is primarily dependent on size and charge. Prior studies have observed increased lymphatic uptake and retentions of over 48 h for negatively charged particles compared to neutral and positively charged particles. We have developed new polymeric materials that extend retention over a more pharmaceutically relevant 7-day period. We used whole body fluorescence imaging to observe in mice the lymphatic trafficking of a series of anionic star poly-(6-*O*-methacryloyl-D-galactose) polymer-NIR dye (IR820) conjugates. The anionic charge of polymers was increased by modifying galactose moieties in the star polymers with succinic anhydride. Increasing anionic nature was associated with enhanced lymphatic uptake up to a zeta potential of ca.−40 mV; further negative charge did not affect lymphatic uptake. Compared to the 20% acid-conjugate, the 40–90% acid-star-polymer conjugates exhibited a 2.5- to 3.5-fold increase in lymphatic uptake in both the popliteal and iliac nodes. The polymer conjugates exhibited node half-lives of 2–20 h in the popliteal nodes and 19–114 h in the deeper iliac nodes. These polymer conjugates can deliver drugs or imaging agents with rapid lymphatic uptake and prolonged deep-nodal retention; thus they may provide a useful vehicle for sustained intralymphatic drug delivery with low toxicity.

1. Introduction

The uptake and distribution of nanoparticles in the lymphatic system is dependent on the size, charge, hydrophobicity, injection site, and the dose of the nanoparticles (Hawley et al., 1995; Porter, 1997; Rao et al., 2010). A number of different delivery vehicles have been employed for lymphatic imaging and drug delivery, including: liposomes, dendrimers, quantum dots, synthetic polymers, and natural polymers. Our laboratory has previously investigated a natural biopolymer, hyaluronan (HA), for targeted lymphatic drug delivery (Cai et al., 2010a, 2008, 2010b,c; Cohen et al., 2009) and determined the optimal particulate size for lymphatic uptake and nodal retention to be 30–50 nm by utilizing *in vivo* fluorescence imaging and fluorophore-labeled polymers.

The effects of size on lymphatic uptake have been well described (Rao et al., 2010), but charge also is an important factor in lymphatic uptake. Negatively charged proteins, liposomes, dendrimers, and PLGA-nanospheres have increased lymphatic uptake compared to neutral to positively charged particles (Kaminskas and Porter, 2011; Patel et al., 1984; Rao et al., 2010; Takakura et al., 1987, 1992); This is due in part to the electrostatic repulsions between the negatively charged particles and the extracellular matrix (Rao et al., 2010), which is primarily negatively charged (Hawley et al., 1995; Porter, 1997; Rao et al., 2010). Also, negatively charged particles are retained longer and to a greater extent by lymph nodes (Kaminskas and Porter, 2011; Patel et al., 1984). However, these studies examined chemically dissimilar particles or proteins, and only one study to date has examined the effect of varying negative charge on lymphatic uptake of otherwise similar particles. Rao and coworkers adjusted the ratio of carboxylic acid terminated poly(D,L-lactic-co-glycolic) in PLGA nanoparticles, and they found that increased negative charge resulted in increased lymphatic uptake during the first 48 h in rats (Rao et al., 2010).

Liposomes, dendrimers, PLGA nanoparticles, and micelles are the most commonly used platforms for lymphatic delivery, and all can be modified with a polyanionic surface to optimize lymphatic uptake. With the exception of PLGA nanoparticles, the uptake of these particles has not been optimized. Also, these technologies are not appropriate for many drug delivery tasks. For example, dendrimers have limited drug loading capacity and may not be biodegradable. Liposomes and micelles can be destabilized in the extravascular

* Corresponding author. Address: 2095 Constant Ave, Lawrence, KS 66047, USA. Fax: +1 785 864 4388.
E-mail address: mforrest@ku.edu (M. Laird Forrest).

0928-0987/$ - see front matter © 2012 Elsevier B.V. All rights reserved.
http://dx.doi.org/10.1016/j.ejps.2012.04.016

space (Proulx et al., 2010). PLGA nanoparticles can be difficult to manufacture and may not sustain the release of small molecule drugs. For these reasons, we developed a new water soluble and degradable star polymer as a lymphatic delivery platform with controlled degrees of anionic charge (Duan et al., 2012). Star polymers are three-dimensional with linear polymeric arms emanating from a branched central core (Cameron and Shaver, 2010; Mendrek and Trzebicka, 2009). Like dendrimers, star polymers are branched polymers that have a compact structure, are globular in shape, and have large surface areas, which make them optimal platforms for lymphatic delivery. Further, hyperbranched polymers and multi-arm star polymers exhibit low intrinsic viscosities and increased solubilities compared to their linear counterparts (Chen et al., 2006; Hult et al., 1999). Star polymers can be synthesized using living radical polymerization techniques to accurately control the molecular weight (Boyer et al., 2009; Gregory and Stenzel, 2011).

A series of 4-armed star-polymers with controlled degrees of negative charge were developed to determine the effect of anionic character on lymphatic uptake. A near infrared dye, IR820, was conjugated to the polymers, so the effects of charge on lymphatic uptake and retention could be measured non-invasively by whole body fluorescent imaging in mice.

2. Experimental

2.1. Materials and methods

Unless noted otherwise, all reagents were ACS grade or better and were purchased from Sigma Aldrich Chemical Co. (St. Louis, MO, USA) or Thermo Fisher Scientific (Waltham, MA, USA). Deuterated solvents for NMR analysis were purchased from Cambridge Isotope Laboratories (Andover, MA, USA). ^{1}H-NMR (400 MHz) and ^{13}C-NMR (100 MHz) spectra were collected on a Bruker DRX 400 spectrometer. Chemical shifts were referenced to δ 7.28 and 77.0 ppm for ^{1}H-NMR and ^{13}C-NMR spectra, respectively. Cell culture media was purchased from Fisher Scientific (Pittsburgh, PA) or ATCC (Manassas, VA, USA). Polyethylene glycol and polystyrene standards were obtained from Scientific Polymer Products (Ontario, NY, USA).

2.2. Star polymer synthesis (star 3)

A series of 4-arm star polymers with controlled degrees of anionic charge, were previously synthesized in our laboratory using the MADIX/RAFT polymerization method. The detailed procedure of the star polymer synthesis and the ^{1}H NMR assignments are reported elsewhere (Duan et al., 2012). Fig. 1A depicts the simplified reaction scheme for the star polymer used herein. The MADIX agent was synthesized using the methods reported by (Stenzel et al., 2004). The MADIX agent was formed by the addition of a xanthate group to pentaerythritol to form the 4-armed core **1** for the star polymer. The MADIX/RAFT polymerization were carried out according to the procedures of (Ting et al., 2009). A 6-*O*-methacryloyl-D-galactose was used as the repeating unit in the polymerization reaction initiated by AIBN to give the sugar–star polymer. After deprotection, the sugar–star polymer **2** (star 2) was modified with various amounts of succinic anhydride to vary the degree of anionic charge on the star polymer. Typically, 20, 40, 60, and 90 wt.% succinic anhydride was mixed with the sugar–star polymer **2** in DMF/pyridine to yield the sugar–acid star polymers **3** with 20, 40, 60, and 90 wt.% acid (star 3–20, star 3–40, star 3–60, and star 3–90), respectively. Structures of the synthesized compounds were verified by ^{1}H-NMR.

The molecular weights and polydispersity index (PDI) of the protected star polymer, poly-(1,2:3,4-*Di*-*O*-isopropylidene-6-*O*-methacryloyl-α-D-galactopyranose), and deprotected star polymer, poly-(6-*O*-methacryloyl-D-galactose) **2**, were determined by size exclusion chromatography (SEC) (Shimadzu 2010CHT) using a TSK gel multipore Hx-M column coupled with a refractive index detector (Shimadzu RID-10A), and using 0.8 ml/min of DMF containing 10-mM LiCl as the mobile phase. Calibration curves were generated with polystyrene standards (1180–339,500 g/mol) or polyethylene glycol (PEG) standards (3070–66,100 g/mol) for the protected and deprotected sugar–star polymers, respectively.

2.3. Star-IR820 synthesis (star 5)

The dye IR-820 was conjugated to the star polymers for *in vivo* imaging (Fig. 1B). First, to a solution of IR-820 (100 mg, 0.094 mmol) in 20 ml of dry DMF, 1,3-diaminopropane (40 μl, 0.47 mmol) was added in one portion. The solution was gradually heated to 60 °C and stirred for 4 h protected from light. The solvent was removed under reduced pressure, and the product was purified by column chromatography (1:1 EtOAC:MeOH). The combined fractions were dried under reduced pressure to yield a dark blue solid **4** (65 mg, 78% yield). The 3-aminopropyl-amino-IR820 **4** was conjugated to the sugar–acid star polymer **3** in dry DMF with EDAC activation and HOBt·H_2O as the catalyst. A cooled solution (0 °C) of the sugar–acid–star polymer **3** (60% acid) (75 mg) in 20 ml dry DMF, EDAC (28.1 mg, 0.147 mmol) and HOBt·H_2O (22.5 mg, 0.147 mmol) were combined. After 5 min, **4** (65 mg, 0.073 mmol) in DMF (5 ml) was added dropwise. The reaction proceeded at ambient temperature overnight and was protected from light. The resulting sugar–acid–star-polymer-IR820 **5** (star 5) was purified by dialysis (10,000 MWCO, Pierce, Rockford, IL, USA) against EtOH:H_2O (1:1) followed by 100% EtOH. Concentration under reduced pressure resulted in a bluish–purple solid. The loading degrees of IR820 on the series of star polymers were determined by ^{1}H NMR in MeOD.

2.4. Rheological properties

The viscosities of the acid star polymers were determined in PBS at pH 7.4. Samples of sugar star polymer (compound **2**) and sugar acid star polymer (compound **3**) were dissolved in PBS (at ca. 100 mg/ml conc.) and dialyzed against PBS (pH 7.4) for 48 h at ambient temperature using a 3.5-kD MWCO dialysis tubing (regenerated cellulose, Fisherbrand) to adjust the pH. The star polymers were then diluted to 1, 5, and 10 mg/ml with PBS (pH 7.4), and the rheological properties were measured in triplicate using an Advanced Rheometer 2000 (TA Instruments, New Castle, DE) at 25 °C using a 40-mm 2° aluminum cone geometry and a 49-μm gap distance. The shear rate was increased using a steady-state flow step from 10 to 100 s^{-1} using 10 points per decade on a log scale and sample periods of 10 s. The steady state parameters were set to 5% deviation for three consecutive points within a maximum time of 1 min per shear rate.

2.5. Zeta potential of the star polymers

Star 2 and star 3 (−20, −40, −60, and −90) polymer (compounds **2** and **3**) samples were dissolved in ddH_2O at a concentration of ca. 1 mg/ml, the pH then was adjusted to 7.2 ± 0.1 with 1-*N* sodium hydroxide, and the final concentration was noted. The samples were diluted to 100 μg/ml with pH 7.25 1-mM phosphate buffer and 1 mM of KCl, and the pH was readjusted if necessary. Zeta potentials were measured on a ZetaPALS (Brookhaven Instruments Corporation, Holtsville, NY, USA) at 20 °C, and the sample measurements were repeated six times. The statistical analysis of the zeta potentials of the star 2 and star 3 polymers was evaluated using a student t-test (GraphPad Prism 4).

Please cite this article in press as: Bagby, T.R., et al. Lymphatic trafficking kinetics and near-infrared imaging using star polymer architectures with controlled anionic character. Eur. J. Pharm. Sci. (2012), http://dx.doi.org/10.1016/j.ejps.2012.04.016

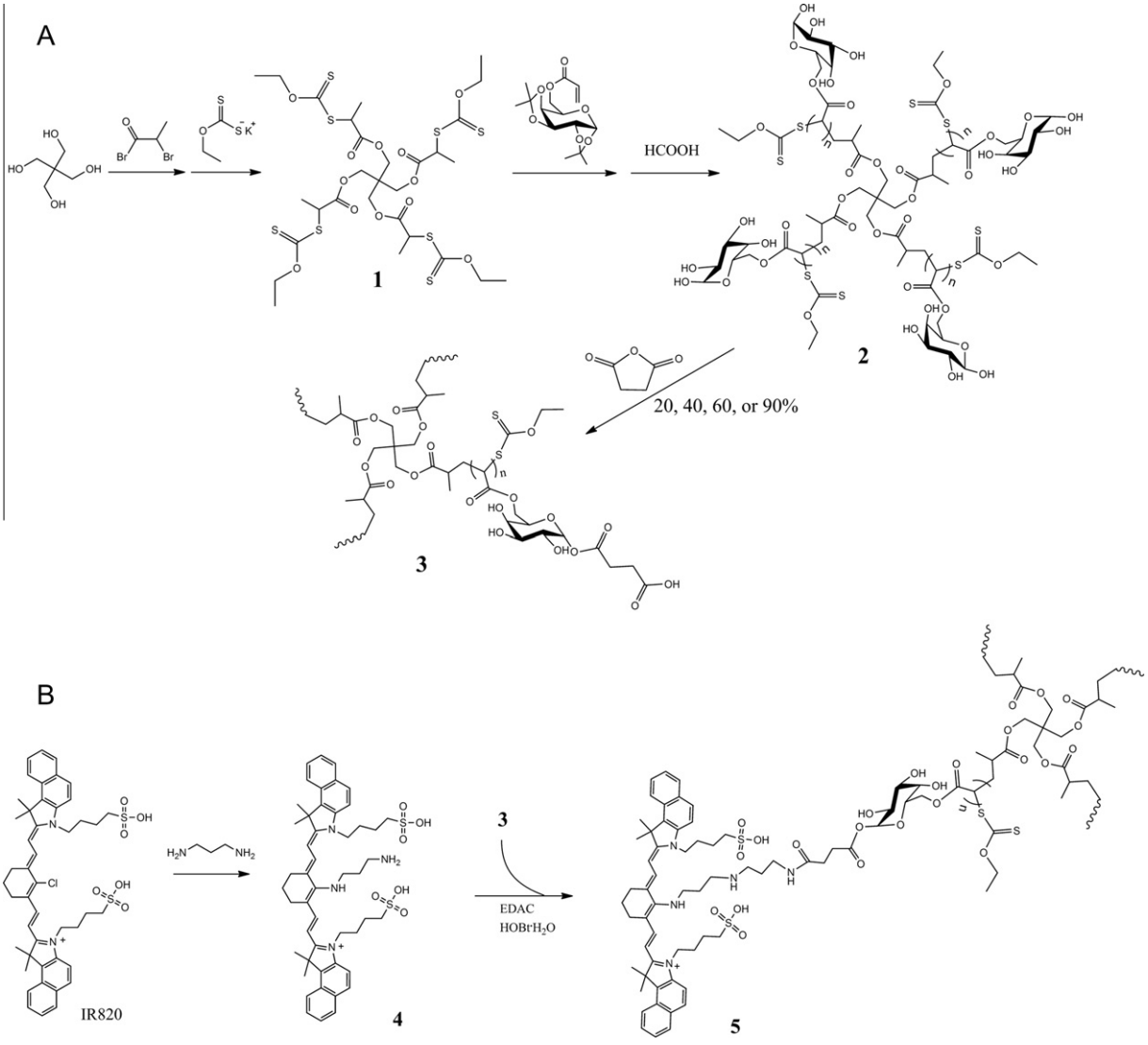

Fig. 1. (A) Synthesis of the 4-arm sugar star polymers **2** by MADIX/RAFT polymerization and the subsequent modification with succinic anhydride to yield the 20%, 40%, 60%, and 90% wt/wt sugar–acid star-polymers **3**. (B) Conjugation of 3-aminopropyl-amino-IR820 **4** to a sugar–acid–star polymer **3** to yield the star-IR820 conjugate **5**.

2.6. Size distribution measurement

Star 2 and star 3 (−20, −40, −60, and −90) polymers were prepared at 0.2 mg/ml in double distilled water. Polymer solutions were filtered through 0.2-μm syringe filters before hydrodynamic radius measurements. The hydrodynamic radius of each polymer solution was determined using a DynaPro™ Plate Reader (Wyatt Technology, Santa Barbara, CA, USA); samples were measured for five acquisitions each consisting of 20 scans per acquisition.

2.7. In vitro toxicity of the star polymers

The cancer cell lines B16F10 (lymphatically metastatic murine melanoma, ATCC, Manassas, VA, USA), MDA-MB-231 (human breast cancer), MDA-1986 (human head and neck squamous cell carcinoma), and HUVEC (normal human endothelial), were maintained in Dulbecco's modified Eagle's medium (DMEM) supplemented with 1% L-Glutamine and 10% bovine growth serum in 5% CO_2 atmosphere. The HER2 expressing murine breast cancer cell line, 4T1.2 Neu, was a gift from Dr. Zhaoyang You of the University of Pittsburg, and the cells were maintained in DMEM supplemented with 1% L-Glutamine, 10% bovine growth serum, and 500 μg/ml of G418 (geneticin) in a 5% CO_2 atmosphere. The lymphatically metastatic human melanoma cell line, A2058, was purchased from ATCC and was maintained in low sodium bicarbonate DMEM (ATCC) supplemented with 1% L-Glutamine and 10% bovine growth serum in a 5% CO_2 atmosphere.

The sugar–acid star polymer (compound **3**) samples (20, 40, 60, and 90 wt.% succination) were dialyzed against PBS (as described in the rheometry section) for 48 h to adjust the pH to 7.4. The solutions were concentrated to ca. 100 mg/ml using a Speedvac concentrator (Labconoco) and diluted in sterile 1 × PBS (Fisher BioReagents, pH 7.4) to eight concentrations between 10^{-4} and 10^{-9} M. Prior to cell growth inhibition studies, cells were trypsinized and seeded at 3000 cells/well in 96-well tissue culture treated plates. After 24 h, the star 3–20, star 3–40, star 3–60, and star 3–90 acid–sugar star polymers (compound **3**) in PBS were added to the HUVEC, A2058, and 4T1.2 Neu cells (n = 8, 10 μl/well, eight concentrations). The star 3–60 sample was further tested in the B16F10, MDA-MB-231, and MDA-1986 cells. A solution of 10% trichloracetic acid was used as a negative control, and media was used as a positive control (n = 8, 10 μl/well). At 72 h post addition, 10 μl of resazurin blue in PBS was added (5-μM final concentration) to each

Please cite this article in press as: Bagby, T.R., et al. Lymphatic trafficking kinetics and near-infrared imaging using star polymer architectures with controlled anionic character. Eur. J. Pharm. Sci. (2012), http://dx.doi.org/10.1016/j.ejps.2012.04.016

well and the well fluorescence was measured after 3 h (λ_{ex}/λ_{em} = 560/590 nm) (SpectraMax Gemini, Molecular Devices, Sunnyvale, CA, USA). IC_{50}'s were determined using the nonlinear regression curve fit for a one-site competition (GraphPad Prism 4, GraphPad Software, La Jolla, CA, USA).

2.8. In vivo imaging of star-IR820 (star 5)

Animals were maintained in sterile housing under the veterinary supervision of the University of Kansas Animal Care Unit. All procedures were approved by the Institutional Animal Care and Use Committee. All mice were fed a low chlorophyll diet (Harlan 2918 irradiated diet, Harlan Laboratories, Indianapolis, IN, USA) for at least one week prior to imaging to decrease food induced organ and skin autofluorescence. The mouse's hair in the area of interest for imaging was removed 24 h prior to imaging with clippers followed by depilatory cream. Female Balb/c mice (20–25 g, Charles River) (3 per group) were anesthetized under isoflurane, placed on a heating pad to maintain normal body temperature, and were injected subcutaneously (s.c.) with 10 μl of a filter-sterilized 0.1-mg/ml (IR820 dye conc.) solution of star 5 conjugates (20%, 40%, 60%, or 90% acid substitution) in the center of the right hind footpad. The mice were imaged from both the dorsal and right sides, both with and without the injection site being covered, for a maximum of 7 days using whole body fluorescence imaging (Cambridge Research and Instrumentation MaestroFlex, Woburn, MA) using an excitation filter of 710–760 nm and broadpass emission filter of 800–950 nm. Animals were not imaged for more than 5 min during any single session.

The intense fluorescence signal from the injection site could saturate the camera, especially during early time points, so it was covered with black tape to improve the dynamic imaging range for the draining lymphatic vessels and lymph nodes. Images were acquired using the autoexposure function, which limits the pixel saturation to <2%, and exposure times were recorded. The use of the autoexposure function resulted in different exposure times for each image, which were normalized by dividing the total counts by the exposure time. The f-stop, camera position, and zoom setting were held constant throughout the studies.

2.9. In vivo imaging data analysis

Images were analyzed using the Maestro software (ver. 2.10). Regions of interest (ROI) were placed over the popliteal and iliac lymph nodes. The total signal (scaled counts/s, see equation below) was recorded for each ROI from both positions (prone and right), and the signal was graphed vs. time. In addition, the area under the curve (AUC) was determined from the total fluorescence intensity vs. time graphs. Significance between multiple groups was determined by one-way ANOVA analysis with a Tukey Multiple Comparisons post-test and student t-tests (GraphPad Prism 4).

$$\text{Scaled counts/s} = \text{counts/full scale} \times 1/\exp(s) \times 1/\text{bin}^2 \times 1/\text{gain}$$

3. Results

3.1. Characterization of the star polymer and star-IR820 conjugates

The synthesis of sugar–star polymers (compound **2**) was verified by mass spectroscopy and NMR (data not shown) (Duan et al., 2012). The molecular weight and PDI were determined by SEC to be 75,000 and 1.132, respectively for the protected sugar–star polymer (reaction intermediate), and 45,000 and 1.15 for the deprotected sugar–star polymer (compound **2**). The IR820 loading degree was determined by ^{1}H NMR in MeOD using the ratio of the aromatic protons of IR820 with the proton on the repeating unit of the star-polymer. The calculated molecular weights and the IR820 loading degrees are presented in Table 1.

Table 1
IR820 loading degree on the various wt.% acid–sugar star polymers (compound **5**).

Polymer	wt.% succination	Polymer MW (kDa)	wt.% IR820	# Dyes/polymer
Star 5–20	20	54	7.8%	5.3
Star 5–40	40	63	6.8%	5.3
Star 5–60	60	72	5.2%	4.6
Star 5–90	90	85.5	8.6%	9.3

3.2. Rheological properties

The effects of size and charge on the rheological properties of the star polymers were determined. The viscosities of the star polymer samples in Fig. 2 represent the apparent viscosities of the polymers at a shear rate of 100 s^{-1}, although the star polymer did appear to undergo minimal shear thinning over the shear rates examined. As the concentration of star polymer was increased the apparent viscosity also increased. However, as the molecular weight increased (star 2 < star 3–20 < star 3–40 < star 3–60 < star 3–90) at a given concentration, the apparent viscosity remained relatively constant (Fig. 2).

3.3. Zeta potential of the star polymers

The zeta potential increased linearly with an increase in wt.% substitution of acid on the star polymers (R^2 = 0.983) (Fig. 3). The zeta potentials of the star polymer samples were determined at

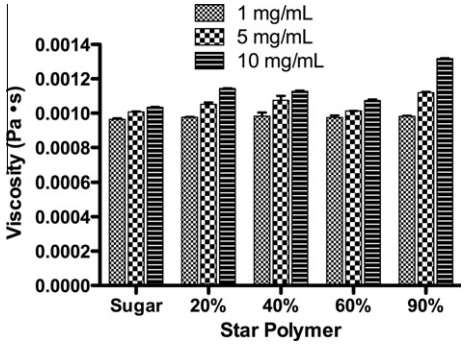

Fig. 2. Viscosity of the sugar–star polymers in pH 7.4 PBS at a shear rate of 100 s^{-1}. (n = 3).

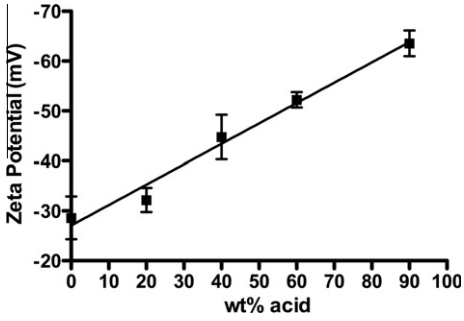

Fig. 3. Zeta potentials of the different wt.% acid sugar star polymers at 20 °C, 100 μg/ml, and a 1-mM phosphate buffer (pH 7.25) with 1-mM KCl. (R^2 = 0.983). Where 0%, 20%, 40%, 60% and 90% acid correspond to the star 2, star 3–20, star 3–40, star 3–60, and star 3–90 polymers, respectively.

Please cite this article in press as: Bagby, T.R., et al. Lymphatic trafficking kinetics and near-infrared imaging using star polymer architectures with controlled anionic character. Eur. J. Pharm. Sci. (2012), http://dx.doi.org/10.1016/j.ejps.2012.04.016

pH 7.4 to ensure that all of the carboxylic acid functional groups were fully ionized (pK_a ca. 4–5), which minimizes effects due to partial protonation of the carboxylic acids. Partial protonation would lead to a reduction in the double layer thickness and zeta potentials of lower magnitude than for fully ionized polymers. Further, the pH studied is indicative of the ionization state *in vivo*, thus the zeta potentials are relevant for the nanoparticles under *in vivo* conditions. The difference in zeta potentials for the star polymers (star 2 and star 3 polymers) were statistically significant with $p < 0.05$ for all pairs of polymers, with the exception of the star 2 (0% acid) vs. star 3–20 and star 3–40 vs. star 3–60, which were not statistically significant.

3.4. Size distribution measurement

The hydrodynamic radii and polydispersities of the sugar star polymers were reported in Table 2. The average diameters of all polymeric nanocarriers ranged approximately from 25 to 50 nm, which meets the size requirement for particle lymphatic uptake.

3.5. In vitro toxicity of the star polymers

All four of the sugar–acid star polymers (star 3–20, star 3–40, star 3–60, and star 3–90) (compounds **3**) had similar low anti-proliferative activity in the cell lines examined including normal and cancer cell lines, with the exception of the star 3–60 (compound **3** derivative containing 60% acid groups) polymer in the MDA-1986 cancer cells. In this case, the star polymer was 10-fold more cytotoxic in MDA-1986 than other lines (Table 3).

3.6. In vivo imaging of star-IR820

In this study, the four star-5 conjugates have identical chemical backbones and a relatively narrow size range, 55 and 85 kDa, but have zeta potentials over a wide range of −28 to −68 mV. The differences in the lymphatic uptake of the star polymers after s.c. administration are expected to be governed primarily by charge rather than size. Drainage from the injection site occurs at similar rates for all four of the star 5 conjugates, as indicated by the same t_{max} (time to reach maximal fluorescence signal) of 0.75–0.83 h (Table 4). In another study by our laboratory with a series of different MW hyaluronan polymers (6.4–697 kD) with the same charge, the t_{max} increased with polymer MW (unpublished data).

The drainage kinetics to the popliteal and iliac nodes of the star 5 conjugates post s.c. administration are presented in Fig. 4 A and B, respectively (Fig. 5). The kinetic profile for the lymphatic drainage of the star 5–20 conjugate to both the popliteal and iliac nodes indicates that the star 5–20 conjugate has statistically lower lymphatic uptake and increased retention in the popliteal and iliac lymph nodes over the length of the study compared to the star 5–40, star 5–60 and star 5–90 acid–star-IR820 conjugates (popliteal node, $p < 0.05$, <0.0001 and <0.001, for the star 5–40, star 5–60 and star 5–90, respectively; iliac node, $p < 0.0001$ for all three conjugates). The star 5–20 conjugate is highly retained at the injection site and the popliteal node, as indicated by the lower maximum fluorescence signal and longer $t_{50\%}$ (time required for the fluorescence signal to reduce by 50%) (Table 4 and Fig. 4A).

Over the first 24 and 6 h, the kinetic profiles for the lymphatic drainage to the popliteal node of the star 5–40 and star 5–90, respectively, conjugates were significantly different than that of the star 5–60 conjugate ($p < 0.05$), as indicated by its significantly shorter $t_{50\%}$ (Fig. 4A and Table 4). Whereas, the star 5–40 and star 5–90 conjugates did not exhibit any significant differences in their lymphatic uptake to the popliteal node, which both have similar $t_{50\%}$ values (Fig. 4A and Table 4). The kinetic profiles for the lymphatic uptake to the iliac node revealed slightly different trends compared to the popliteal node. The star 5–90 conjugate profile was statistically different than the star 5–40 and star 5–60 conjugates over the first 24 and 50 h, respectively ($p < 0.05$), in that the star 5–90 conjugate exhibited the shortest t_{max} and a longer $t_{50\%}$ than for the star 5–40 and star 5–60 conjugates which had similar $t_{50\%}$ and t_{max} values Fig. 4B and Table 4).

The star 5–40, star 5–60 and star 5–90 acid–star-IR820 conjugates exhibit remarkably different nodal retentions in the popliteal and iliac lymph nodes. The star 5–60 conjugate cleared rapidly from the popliteal node compared to the other conjugates as indicated by the short $t_{50\%}$ ($p < 0.05$, Table 4), but was retained in the iliac node for almost a day. In contrast, the star 5–40 and star 5–90 conjugates have similar popliteal $t_{50\%}$ values of ca. 4 h ($p < 0.001$), but the star 5–90 conjugate was retained two times longer in the iliac node in comparison with star 5–40 and star 5–60 conjugates (Table 4). Further, the star 5–20 conjugate was highly retained in both the popliteal and iliac nodes compared to its more anionic counterparts as demonstrated by its longer $t_{50\%}$

Table 2
Hydrodynamic radius and polydispersity measurements of sugar star polymers with 0%, 20%, 40%, 60% and 90% wt acid modification (star 2–0, star 3–20, star 3–40, star 3–60, and star 3–90). Values were reported as mean ± standard deviation.

Polymer	Hydrodynamic radius mean ± std. (nm)	Polydispersity mean ± std. (%)
Star 2–0	12.2 ± 0.8	49.8 ± 12.6
Star 3–20	24.1 ± 2.8	57.1 ± 0.0
Star 3–40	10.8 ± 0.4	57.1 ± 0.0
Star 3–60	13.9 ± 0.3	57.1 ± 0.0
Star 3–90	19.5 ± 4.3	57.1 ± 0.0

Table 4
The t_{max} and $t_{50\%}$ values for the popliteal and iliac lymph nodes after s.c. administration of the star 5 conjugates (compound 5) in the right hind footpad of mice.

	Popliteal		Iliac	
wt.% Acid	t_{max} (h)	$t_{50\%}$ (h)	t_{max} (h)	$t_{50\%}$ (h)
Star 5–20	0.75–0.83	20 ± 6	1	114 ± 28
Star 5–40	0.75–0.83	4.9 ± 0.3	2	19 ± 10
Star 5–60	0.75–0.83	1.9 ± 0.6	1	19 ± 6
Star 5–90	0.75–0.83	3.4 ± 0.3	0.5	40 ± 16

Table 3
IC_{50} values of the various wt.% acid star 3 polymers (compound **3**) in various cell lines post 72 h incubation.

Polymer/cell line	Star 3–20	Star 3–40	Star 3–60	Star 3–90
HUVEC	~50 μM (2.7 mg/ml)	~55 μM (3.5 mg/ml)	~100 μM (7.2 mg/ml)	~55 μM (4.7 mg/ml)
A2058	~50 μM (2.7 mg/ml)	~40 μM (2.5 mg/ml)	~60 μM (4.3 mg/ml)	~50 μM (4.3 mg/ml)
4T1.2 Neu	~50 μM (2.7 mg/ml)	~50 μM (3.2 mg/ml)	~100 μM (7.2 mg/ml)	~55 μM (4.7 mg/ml)
B16F10	–	–	>100 μM (7.2 mg/ml)	–
MDA1986	–	–	10 μM (0.72 mg/ml)	–
MDA-MB-231	–	–	⩾100 μM (7.2 mg/ml)	–

Please cite this article in press as: Bagby, T.R., et al. Lymphatic trafficking kinetics and near-infrared imaging using star polymer architectures with controlled anionic character. Eur. J. Pharm. Sci. (2012), http://dx.doi.org/10.1016/j.ejps.2012.04.016

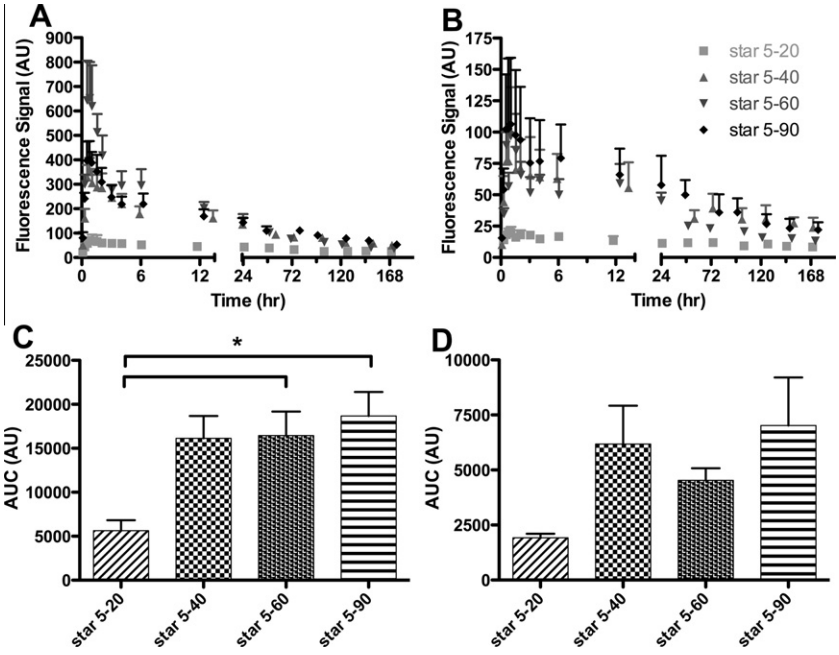

Fig. 4. Star-IR820 (star 5 conjugates) drainage to the popliteal (A & C) and iliac (B & D) lymph nodes. Drainage kinetics to the (A) popliteal and (B) iliac lymph nodes after s.c. administration into the right hind footpad. Area under the curve (AUC) of the acid–star-IR820 conjugates in the (C) popliteal and (D) iliac lymph nodes. (AU = Arbitrary Units) (*$p = 0.0194$).

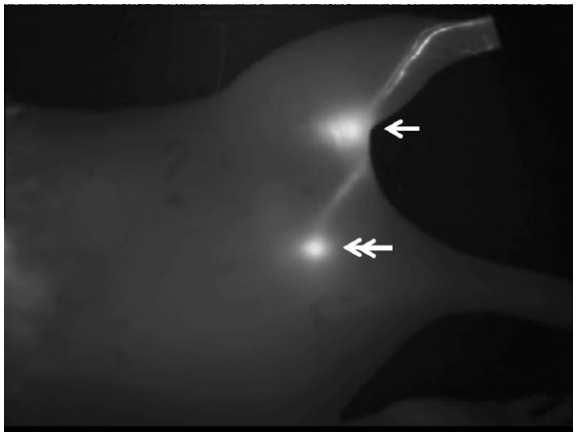

Fig. 5. Representative fluorescent imaging of mouse lymphatics after injection of the star 5–60 conjugate in the hind footpad 1 h post injection. Arrow: popliteal node, double-arrow: iliac node.

values ($p < 0.05$). However, the distribution of the AUC for the different degrees of anionic charge was similar for both the popliteal and iliac nodes (Figs. 4C and D). The star 5–40, star 5–60, and star 5–90 conjugates exhibited a 2.5- to 3.5-fold increase in the lymphatic uptake compared to the star 5–20 conjugate for both the popliteal and iliac nodes ($p < 0.05$, student t-test, star 5–20 vs. star 5–40 (popliteal), star 5–60 (popliteal and iliac), and star 5–90 (popliteal)).

We imaged mice from both right and dorsal sides to assess drainage into the popliteal and iliac nodes. The same trends were observed for both imaging positions, but the right side was used for analysis as it produced greater signal intensities and a higher signal to noise ratio compared to the dorsal or ventral positions. The ventral position resulted in a decrease in the signal to noise ratio due to the increased autofluorescence contributions of the organs in the abdomen. In addition, the iliac node was not visualized while imaging in the ventral position due to its increased depth in this position. Both the lymph nodes and draining lymphatic vessels were clearly visualized against the background tissues using fluorescence imaging (Fig. 5). Due to limitations of *in vivo* fluorescence imaging, only shallow nodes were identified; further drainage past the iliac node of these star 5 conjugates is possible.

4. Discussion

Compared to linear polymers, star polymers are better optimized for lymphatic imaging and drug delivery due to their inherent low viscosities, increased solubility, decreased solution entanglement, and enhanced thermodynamic properties (Cameron and Shaver, 2010; Hult et al., 1999; Qiu and Bae, 2006). Within the concentration range appropriate for drug delivery, the apparent viscosities of the star polymer were virtually independent of increases in drug concentration and molecular weight. Compared to the viscosity of water, which is 0.001 Pa·s, at 20 °C, the observed viscosities of the star polymers were ca. 0.001–0.0012 Pa s, which are insignificant differences in viscosity in practice.

In addition to size, particle charge plays a critical role in lymphatic uptake, retention, and disposition (Patel et al., 1984; Rao et al., 2010; Takakura et al., 1987, 1992). After subcutaneous administration of negatively charged particles, they are readily drained into lymphatics from the interstitium due to the electrostatic repulsions between the negatively charged particles and the extracellular space (Rao et al., 2010). Conversely positively charged particles drain more slowly from the injection site due to the attractive forces between the particles and the negatively charged matrix. Zeta potential (ζ) can be used to measure the ionic nature of nanoparticles zeta potential greater than 30 mV indicates a strongly cationic particle, between +10 and −10 mV is considered to be a neutral particle, and less than −30 mV indicates a strongly anionic particle (Clogston and Patri, 2011).

The correlation between star polymer zeta potential and percent substitution of succinic anhydride allows for comparisons of the lymphatic uptake of the acid–star polymers with other

polymeric systems. Rao et al., 2010 developed a series of PLGA-PMA:PLGA–COOH nanoparticles with an increasing ratio of PLGA–COOH to PLGA-PMA to increase the anionic character, resulting in an increase in zeta potential from −44.6 ± 11.3 mV to −57.1 ± 11.1 mV (an increase of their absolute values). As the zeta potential increased, an increase in the lymphatic uptake was observed. A 4.7-fold increase in the nanoparticle concentration in the popliteal node and a 10.1-fold increase in the cumulative nodal uptake (combination of the popliteal, internal inguinal, iliac, and renal lymph nodes) were observed for the −57.1 mV (20:80 PLGA-PMA:PLGA–COOH) nanoparticles.

Intralymphatic drug delivery vehicles should be optimized not only for size, but also for charge to speed lymphatic uptake and enhance nodal retention after subcutaneous administration. Cationic particles show slowest injection site drainage after s.c. injection, are poorly retained by the lymph nodes, have increased toxicity, liver accumulation, and have a high propensity for macrophages engulfment (Hawley et al., 1997; Jain et al., 2010; McNerny et al., 2010; Patel et al., 1984; Takakura et al., 1992). In contrast negatively charged particles exhibit enhanced lymphatic uptake, increased nodal retention, and decreased toxicity.

Toxicity both *in vitro* and *in vivo* is highly important in developing synthetic polymers for enhanced lymph node retention. Cationic dendrimers exert their toxicity by interacting with the negatively charged lipid bilayer, resulting in destabilization of the cellular membrane (Jain et al., 2010; McNerny et al., 2010). The star polymers do not exhibit significant toxicity *in vitro* when compared to similar poly-ionic polymers currently used for drug and gene delivery (IC_{50} ca. 5 mg/ml). For example, the star polymers **3** are 100-fold less toxic than most cationic dendrimers and PEI used for drug and gene delivery. Peng et al., 2008 demonstrated that chlorin-core star block m-PEG-b-PCL copolymer micelles exhibited no observable toxicity against MCF-7 breast cancer cells after 24 h incubation at the highest concentration of 500 μM (Peng et al., 2008), which is similar to our star polymers (IC_{50} ca. 50–100 μM).

While the star 5–40, star 5–60, and star 5–90 polymers all exhibit similar cumulative lymphatic uptake, the star 5–60 conjugate had more favorable characteristics of rapid drainage from the popliteal lymph node coupled with long retention in the iliac node. The sugar moiety in the repeating unit of the star polymer was included primary to enhance solubility, and the addition of saccharides to liposomes has been reported to enhance lymphatic uptake and nodal retention (Wu et al., 1981). The sugars also substantially decreased the toxicity of these polymers and enhanced biocompatibility. Similar acid star polymers made without the sugar moiety (data not shown) were considerably more toxic *in vitro* and *in vivo*.

The star polymers did not exert any visible signs of toxicity or adverse effects over the 7 day kinetic study at concentrations as high as 0.7-mg/kg star 5 conjugate. In addition, study animals have been monitored for up to 6 months after injection with no visual indication of poor health or reduction in normal growth rate. Nano-sized particles can exert considerable chronic toxicity with no acute *in vivo* or *in vitro* toxicity. Chen et al. reported that gold nanoparticles less than 5 nm and greater than 50 nm were non-toxic after intraperitoneal injection; however, particles of 8–37 nm caused death within 3 weeks (Chen et al., 2009). The study concluded the toxicity was due to non-immunogenicity of the particles, and the addition of immunogenic peptides made the nanoparticles tolerable. The star polymers were given subcutaneously, which may substantially increase the exposure to the immune surveyance system due to preferential accumulation in the lymph nodes. In addition, the star polymers incorporate biodegradable ester linkages in the arms, which may improve clearance of the material as the arms disconnect from the core.

5. Conclusions

We developed a new star-polymer with controlled degrees of anionic charge for lymphatic imaging and drug delivery. The star-polymer platform displays similar characteristics to dendrimers, but its synthesis is more straightforward and cost effective. In addition, this platform exhibited significantly reduced toxicities compared to conventional dendrimers such as PAMAM. Star polymers exhibit similar lymphatic uptake and trafficking characteristics to endogenous polysaccharide, such as HA, but are significantly less viscous and easily functionalized with drug or dyes. Further, the star polymer platform provides a compact, low polydispersity carrier with numerous functional groups for conjugation. Finally, we were able to optimize for rapid lymphatic uptake and prolonged deep-nodal retention.

The star polymers were highly retained within the iliac node compared to the popliteal node, suggesting that the star polymer platform may be beneficial for treatment of the deep lymphatics where metastases in the echelon nodes are present. The star polymers could be used as treatment carriers for locally advanced metastatic cancers with the involvement of two or more lymph nodes. The rapid drainage of the star 5–40, star 5–60, and star 5–90 polymer conjugates could minimize the local release of chemotherapeutics at the injection site due to their rapid drainage from the injection site and enhanced lymphatic uptake relative to the star 5–20 polymer. Additionally, the acid-star polymers **3** would be ideal carriers for vesicating drug conjugates, since the carriers are rapidly trafficked from the injection site to the deeper lymph nodes. Currently, we are developing anti-cancer drug conjugates of the star polymers for the treatment of regionally metastatic cancers.

Acknowledgements

This work was supported by awards from the American Cancer Society (RSG-08-133-01-CDD), the Susan G. Komen Foundation (KG090481), a Pfizer Predoctoral Scholarship to TRB, and a PhRMA Foundation Predoctoral Fellowship to TRB. Also, the authors would like to thank Dr. Sarah Kieweg and Thora Whitmore for the use of the Advanced Rheometer 2000. TRB performed imaging studies and SD characterized and synthesized the materials; their contributions and authorship were equal in this study.

References

Boyer, C., Bulmus, V., Davis, T.P., Ladmiral, V., Liu, J., Perrier, S., 2009. Bioapplications of RAFT polymerization. Chem. Rev. 109, 5402–5436.

Cai, S., Xie, Y., Bagby, T.R., Cohen, M.S., Forrest, M.L., 2008. Intralymphatic chemotherapy using a hyaluronan-cisplatin conjugate. J. Surg. Res. 147, 247–252.

Cai, S., Thati, S., Bagby, T.R., Diab, H.M., Davies, N.M., Cohen, M.S., Forrest, M.L., 2010a. Localized doxorubicin chemotherapy with a biopolymeric nanocarrier improves survival and reduces toxicity in xenografts of human breast cancer. J. Control Release 146, 212–218.

Cai, S., Xie, Y., Davies, N.M., Cohen, M.S., Forrest, M.L., 2010b. Carrier-based intralymphatic cisplatin chemotherapy for the treatment of metastatic squamous cell carcinoma of the head & neck. Ther. Deliv. 1, 237–245.

Cai, S., Xie, Y., Davies, N.M., Cohen, M.S., Forrest, M.L., 2010c. Pharmacokinetics and disposition of a localized lymphatic polymeric hyaluronan conjugate of cisplatin in rodents. J. Pharm. Sci. 99, 2664–2671.

Cameron, D.J.A., Shaver, M.P., 2010. Aliphatic polyester polymer stars: synthesis, properties and applications in biomedicine and nanotechnology. Chem. Soc. Rev. 40, 1761–1776.

Chen, Y., Shen, Z., Barriau, E., Kautz, H., Frey, H., 2006. Synthesis of multiarm star poly(glycerol)-block-poly(2-hydroxyethyl methacrylate). Biomacromolecules 7, 919–926.

Chen, Y.S., Hung, Y.C., Liau, I., Huang, G.S., 2009. Assessment of the *in vivo* toxicity of gold nanoparticles. Nanoscale Res. Lett. 4, 858–864.

Clogston, J.D., Patri, A.K., 2011. Zeta potential measurement. Methods Mol. Biol. 697, 63–70.

Please cite this article in press as: Bagby, T.R., et al. Lymphatic trafficking kinetics and near-infrared imaging using star polymer architectures with controlled anionic character. Eur. J. Pharm. Sci. (2012), http://dx.doi.org/10.1016/j.ejps.2012.04.016

Cohen, M.S., Cai, S., Xie, Y., Forrest, M.L., 2009. A novel intralymphatic nanocarrier delivery system for cisplatin therapy in breast cancer with improved tumor efficacy and lower systemic toxicity *in vivo*. Am. J. Surg. 198, 781–786.

Duan, S., Cai, S., Yang, Q., Forrest, M.L., 2012. Multi-arm polymeric nanocarrier as a nitric oxide delivery platform for chemotherapy of head and neck squamous cell carcinoma. Biomaterials 33, 3243–3253.

Gregory, A., Stenzel, M.H., 2011. The use of reversible addition fragmentation chain transfer polymerization for drug delivery systems. Expert opin. drug deliv. 8, 237–269.

Hawley, A.E., Davis, S.S., Illum, L., 1995. Targeting of colloids to lymph-nodes – influence of lymphatic physiology and colloidal characteristics. Adv. Drug Deliv. Rev. 17, 129–148.

Hawley, A.E., Illum, L., Davis, S.S., 1997. Lymph node localisation of biodegradable nanospheres surface modified with poloxamer and poloxamine block co-polymers. FEBS Lett. 400, 319–323.

Hult, A., Johansson, M., Malmström, E., 1999. Hyperbranched polymers. In: Roovers, J. (Ed.), Branched Polymers II. Springer, Berlin/Heidelberg, pp. 1–34.

Jain, K., Kesharwani, P., Gupta, U., Jain, N.K., 2010. Dendrimer toxicity: Let's meet the challenge. Int. J. Pharm. 394, 122–142.

Kaminskas, L.M., Porter, C.J., 2011. Targeting the lymphatics using dendritic polymers (dendrimers). Adv. Drug Deliv. Rev. 63, 890–900.

McNerny, D.Q., Leroueil, P.R., Baker, J.R., 2010. Understanding specific and nonspecific toxicities: a requirement for the development of dendrimer-based pharmaceuticals. Wiley Interdiscip. Rev. Nanomed. Nanobiotechnol. 2, 249–259.

Mendrek, B., Trzebicka, B., 2009. Synthesis and characterization of well-defined poly(tert-butyl acrylate) star polymers. Eur. Polym. J. 45, 1979–1993.

Patel, H.M., Boodle, K.M., Vaughan-Jones, R., 1984. Assessment of the potential uses of liposomes for lymphoscintigraphy and lymphatic drug delivery. Failure of 99m-technetium marker to represent intact liposomes in lymph nodes. Biochim. Biophys. Acta 801, 76–86.

Peng, C.-L., Shieh, M.-J., Tsai, M.-H., Chang, C.-C., Lai, P.-S., 2008. Self-assembled star-shaped chlorin-core poly(…õ-caprolactone), Äìpoly(ethylene glycol) diblock copolymer micelles for dual chemo-photodynamic therapies. Biomaterials 29, 3599–3608.

Porter, C.J., 1997. Drug delivery to the lymphatic system. Crit. Rev. Ther. Drug Carrier Syst. 14, 333–393.

Proulx, S.T., Luciani, P., Derzsi, S., Rinderknecht, M., Mumprecht, V., Leroux, J.C., Detmar, M., 2010. Quantitative imaging of lymphatic function with liposomal indocyanine green. Cancer Res. 70, 7053–7062.

Qiu, L.Y., Bae, Y.H., 2006. Polymer architecture and drug delivery. Pharm. Res. 23, 1–30.

Rao, D.A., Forrest, M.L., Alani, A.W., Kwon, G.S., Robinson, J.R., 2010. Biodegradable PLGA based nanoparticles for sustained regional lymphatic drug delivery. J. Pharm. Sci. 99, 2018–2031.

Stenzel, M.H., Davis, T.P., Barner-Kowollik, C., 2004. Poly(vinyl alcohol) star polymers prepared via MADIX/RAFT polymerisation. Chem. Commun. (Camb), 1546–1547.

Takakura, Y., Atsumi, R., Hashida, M., Sezaki, H., 1987. Development of a novel polymeric prodrug of mitomycin C, mitomycin C-dextran conjugate with anionic charge. II. Disposition and pharmacokinetics following intravenous and intramuscular administration. Int. J. Pharm. 37, 145–154.

Takakura, Y., Hashida, M., Sezaki, H., 1992. Lymphatic transport after parenteral drug administration. In: Charman, W.N., Stella, V.J. (Eds.), Lymphatic Transport of Drugs. CRC Press, Boca Raton, pp. 255–278.

Ting, S.R., Gregory, A.M., Stenzel, M.H., 2009. Polygalactose containing nanocages: the RAFT process for the synthesis of hollow sugar balls. Biomacromolecules 10, 342–352.

Wu, M.S., Robbins, J.C., Bugianesi, R.L., Ponpipom, M.M., Shen, T.Y., 1981. Modified *in vivo* behavior of liposomes containing synthetic glycolipids. Biochim. Biophys. Acta 674, 19–29.

Please cite this article in press as: Bagby, T.R., et al. Lymphatic trafficking kinetics and near-infrared imaging using star polymer architectures with controlled anionic character. Eur. J. Pharm. Sci. (2012), http://dx.doi.org/10.1016/j.ejps.2012.04.016